

TESTING A SCALE-INDEPENDENT METHOD TO MEASURE THE MASS OF BLACK HOLES

M. GLIOZZI

George Mason University, 4400 University Drive, Fairfax, VA 22030

L. TITARCHUK

George Mason University, 4400 University Drive, Fairfax, VA 22030

S. SATYAPAL

George Mason University, 4400 University Drive, Fairfax, VA 22030

D. PRICE

George Mason University, 4400 University Drive, Fairfax, VA 22030

I. JANG

George Mason University, 4400 University Drive, Fairfax, VA 22030

Draft version October 31, 2018

ABSTRACT

Estimating the black hole mass at the center of galaxies is a fundamental step not only for understanding the physics of accretion, but also for the cosmological evolution of galaxies. Recently a new method, based solely on X-ray data, was successfully applied to determine the black hole mass in Galactic systems. Since X-rays are thought to be produced via Comptonization process both in stellar and supermassive black holes, in principle, the same method may be applied to estimate the mass in supermassive black holes. In this work we test this hypothesis by performing a systematic analysis of a sample of AGNs, whose black hole mass has been already determined via reverberation mapping and which possess high quality XMM-Newton archival data. The good agreement obtained between the black hole masses derived with this novel scaling technique and the reverberation mapping values suggests that this method is robust and works equally well on stellar and supermassive black holes, making it a truly scale-independent technique for black hole determination.

Subject headings: Galaxies: active – Galaxies: nuclei – X-rays: galaxies

1. INTRODUCTION

There is now convincing evidence that the most powerful persistent sources in our Galaxy (Galactic black hole systems; hereafter GBHs) and in the universe at large (active galactic nuclei; AGNs) are powered by gravitational accretion onto stellar and supermassive black holes, respectively. One of the most evident manifestations of black hole systems (BHs) is the presence of relativistic jets, which may have a huge impact on their environment over distances that are well beyond the radius of influence of the black hole itself, as demonstrated by recent work on the effects of powerful jets at the center of galaxy clusters (e.g. McNamara et al. 2000; Fabian et al 2003). In addition, and perhaps more importantly, the tight correlations found between the BH mass (M_{BH}) and several galaxy parameters such as the velocity dispersion or the mass of the bulge (e.g. Gebhardt et al. 2000; Ferrarese & Merritt 2000) clearly demonstrate that black hole growth and the build-up process of galaxies are closely related and therefore black holes are essential ingredients in the evolution of galaxies.

The estimate of the mass of supermassive black holes at the center of galaxies is the most crucial parameter needed to understand the formation and evolution processes in galaxies as well as the central engine in AGNs. Different methods have been developed to mea-

sure M_{BH} in AGNs, depending on their characteristics (e.g., degree of activity, variability, distance). For example, in the case of weakly active or quiescent galaxies, M_{BH} can be determined by directly modeling the dynamics of gas or stars in the vicinity of the black hole (e.g. Kormendy & Richstone 1995; Magorrian et al. 1998). On the other hand, for highly active broad-lined galaxies that show strong variability, the most widely used way to estimate M_{BH} relies upon a technique known as reverberation mapping (e.g., Peterson et al. 2004 and references therein; see Czerny & Nikolaïjuk 2010 for a recent review of the most commonly used methods).

Mass estimates obtained by these methods have provided very important results for our understanding of BH formation and galaxy evolution. However, all methods have specific limitations. For example, methods based on the modeling of gas and stellar dynamics require the sphere of influence of the BH to be resolved. Therefore, these techniques can successfully be applied only to nearby galaxies with relatively massive BHs and where the galaxy's optical emission is not substantially affected by the black hole activity. On the other hand, the reverberation method is time intensive, and cannot be applied to very luminous sources, whose variability is typically characterized by small-amplitude flux changes occurring on very long timescales. Furthermore, this technique re-

quires the presence of a detected broad line region (BLR), whose nature and geometry is still poorly known. Similar limitations affect most of the secondary methods, which rely on some empirical relationship between M_{BH} and different properties of the host galaxy (see Vestergaard 2009 for a recent review). Additionally, bright type 1 AGNs (i.e. the AGNs characterized by the presence of a BLR) comprise only a small minority of the total galaxy population, severely limiting the number of galaxies that can be probed with this technique. Indeed, even amongst the population of known optically-identified AGNs, type 2 AGNs (i.e., the AGNs without visible BLR) appear to be about 4 times more numerous than type 1 AGN (Maiolino & Rieke 1995).

Exploring the SMBH mass function in as diverse as possible galactic environments is essential to understand the evolutionary history of BHs and their connection to their host galaxies. To address this serious deficiency, it is critical to explore alternative methods to determine the BH mass that are not dependent on measurements at optical wavelengths.

X-ray observations are one of the most effective means to investigate the properties of AGNs for several reasons. First, the X-ray emission is one of the defining properties of AGNs: while optical lines generally attributed to AGN activity may be obscured, suppressed, or undetected for several different reasons (e.g., low signal-to-noise ratio S/N, excessive redshift, galaxy or star light contamination), the X-ray emission appears to be ubiquitous in AGNs. Second, the X-rays are produced and reprocessed in the inner, hottest nuclear regions of the source. Therefore, unlike the optical lines from the broad and narrow line regions that are produced by the reprocessing of the primary emission, the X-ray emission directly traces the black hole activity. Finally, the penetrating power of (hard) X-rays allows them to carry information from the inner core regions without being substantially affected by absorption.

At first order, from the spectral point of view, the AGN X-ray emission in the 2–10 keV energy range is adequately described by a simple power-law model. Importantly, the photon index Γ appears to correlate directly with the accretion rate, suggesting that X-ray spectral properties provide indirect information on the accretion state in AGNs. While there is growing evidence of a positive correlation between Γ and Eddington ratio for bright AGNs (e.g. Shemmer et al. 2006; Papadakis et al. 2009), there is also suggestive evidence of a possible anti-correlation for BH systems accreting at low Eddington ratio (e.g. Constantin et al. 2009; Wu & Gu 2008). Although several details are still unknown, it is now widely accepted that the bulk of the X-ray emission both in AGNs and GBHs is produced by the Comptonization process, i.e. the repeated inverse Compton scattering, where seed photons likely produced via thermal emission by an accretion disk are up-scattered by highly energetic electrons. Therefore, X-rays represent one of the most effective tools to probe the properties of black holes systems and may provide independent constraints on their mass.

In this work we investigate whether a novel method to estimate M_{BH} , which is based solely on X-ray spectral data and was successfully applied to GBHs by Shaposhnikov & Titarchuk (2009; hereafter ST09), can be

extended to AGNs. To this end, we utilize a sample of AGNs with M_{BH} already well constrained via reverberation mapping and with good-quality X-ray data. In Section 2 we summarize the main characteristics of this method. The AGN sample and the data reduction are described in Section 3. The results are presented in Section 4 and discussed in Section 5, where we draw our main conclusions.

2. A NEW METHOD TO ESTIMATE M_{BH}

Recently Shaposhnikov & Titarchuk (2009) carried out an extensive and systematic analysis of the temporal and spectral X-ray data from 17 spectral transition episodes in 8 different GBHs. Their main findings can be summarized as follows: (1) Two positive correlations are found: the first one involving temporal and spectral properties and specifically relating the quasi periodic oscillation (QPO) frequency and the photon index Γ ; the second one relating two spectral parameters of a specific Comptonization model described below: the normalization N_{BMC} and Γ . (2) Both spectral evolution trends (QPO - Γ and N_{BMC} - Γ) can be adequately parametrized by analytical functions, which are similar for the different GBHs. (3) The self-similarity of these pair of trends in different GBHs allows the estimate of M_{BH} and distance for these binary systems.

Since the Comptonization process producing the X-ray emission is widely thought to work in the same way in stellar and supermassive black holes, in principle, the same method may be applied to estimate the mass of supermassive black holes. Clearly, it is not possible to use the QPO - Γ diagram, since no firm detections of QPOs have been reported in AGNs (with the exception of the NLS1 RE J1034+396 in one occasion; Gierliński et al. 2008). But this does not represent a problem for AGNs, since their distance is independently and robustly determined from redshift measurements or from variable star methods for objects of the Local Group. Hereafter, we will therefore focus solely on the N_{BMC} - Γ diagram.

In the following, we first describe the general details of the Comptonization model used to fit the X-ray spectra and the basic characteristics of the scaling method that allows one to estimate the mass for any BH system by simply scaling the M_{BH} value from a suitable Galactic reference source.

2.1. The BMC model

Although the geometry and nature of the Comptonizing region are still matter of debate because of spectral degeneracy, for our purpose (i.e. estimating black hole masses), the specific physical condition of the Comptonizing medium (i.e. energy and spatial distribution of the upscattering electrons and their optical depth) are negligible, provided that the Comptonization process is characterized in a simple, general, yet physically correct way. These criteria are met by the so called Bulk Motion Comptonization model (BMC), which is a generic Comptonization model able to describe equally well the thermal Comptonization (i.e. the inverse Compton scattering produced by electrons with a Maxwellian energy distribution) and the bulk motion Comptonization (where the seed photons are scattered off electrons with bulk relativistic motion), although it was historically developed

to describe the Comptonization of thermal seed photons by a relativistic converging flow (Titarchuk et al. 1997).

The BMC model is characterized by 4 free parameters: 1) the temperature of the thermal seed photons kT , 2) the energy spectral index α (which is related to the photon index by the relation $\Gamma = 1 + \alpha$), 3) a parameter $\log(A)$ related to the Comptonization fraction f (i.e., the ratio between the number of Compton scattered photons and the number of seed photons) by the relation $f = A/(1 + A)$, and 4) the normalization N_{BMC} .

In simple words, the BMC model (which is implemented in the spectral fitting package `Xspec`) convolves the thermal seed photons and a generic Comptonization Green's function producing a power law. As a consequence, this spectral model generally provides a good fit for X-ray spectra of accreting black holes, since their continuum is adequately described by a power law.

The BMC model presents two important advantages with respect to the power-law model (PL), which is often used to parametrize the Comptonization component: 1) Unlike the PL, which is a phenomenological model, the BMC parameters are computed in a self-consistent way; 2) Unlike the PL, the power law produced by BMC does not extend to arbitrarily low energies and thus does not affect the normalization of the thermal component nor the amount of local absorption, which is often present around accreting objects.

2.2. A new scaling method

Generally, during their transitions from the low-hard (LH) to the high-soft (HS) spectral state different GBHs show similar spectral variability patterns. Specifically, when the X-ray spectra are fitted with the BMC model, and Γ is plotted versus N_{BMC} , the spectral evolution appears to be characterized by two saturation levels (the lower one corresponding to the LS and the higher one to the HS) connected by a monotonically increasing curve. Following ST09, this spectral trend can be parameterized by the following functional form:

$$\Gamma(N_{\text{BMC}}) = A - B \ln \left\{ \exp \left[1 - (N_{\text{BMC}}/N_{\text{tr}})^\beta \right] + 1 \right\} \quad (1)$$

Note that ST09 provide in their Equation (10) a slightly different functional form that comprises an additional parameter D in order to be able to fit both the QPO - Γ and N_{BMC} - Γ trends. However, since $D = 1$ for the pattern of our interest, Equation (1) coincides with Eq.(10) of ST09.

By virtue of the similarity of these N_{BMC} - Γ trends among GBHs, the value of M_{BH} (and the distance, when the N_{BMC} - Γ plot is used in combination with the QPO - Γ plot) of any GBH can be obtained from a direct scaling process. Simply speaking, if M_{BH} (and the distance) is known for a suitable GBH considered as a reference system, the black hole mass for any other GBH can be determined by horizontally shifting its self-similar function until it matches the reference object's pattern (a visual explanation of this scaling process is provided in Section 3 when this technique is applied to AGNs).

The physical basis of these scaling techniques is thoroughly explained by ST09 and essentially relies on few reasonable considerations that can be summarized as follows: (1) the QPO frequency is inversely proportional to M_{BH} (which can be readily understood considering that the larger M_{BH} , the larger the distance from the BH

of the accretion inflow responsible for the radiation, and hence the longer the dynamical timescale of the process); (2) the BMC normalization is a function of luminosity and distance: $N_{\text{BMC}} \propto L/d^2$ (by definition of the BMC model); (3) the luminosity of an accreting black hole system can be expressed as $L \propto \eta M_{\text{BH}} \dot{m}$, where η is the radiative efficiency and \dot{m} the accretion rate in Eddington units. The self-similarity of the N_{BMC} - Γ correlation implies that, in the same spectral state, different sources have similar values of η and \dot{m} . Therefore, the photon index is a reliable indicator for the source's spectral state independently of its BH mass.

In simple terms, the necessary steps to derive M_{BH} with this method can be summarized as follows:

- (1) Construct a $\Gamma - N_{\text{BMC}}$ plot for a GBH of known mass and distance, which will be used as reference (hereafter denoted by the subscript r) and for a target of interest (denoted by the subscript t).
- (2) Infer the normalization ratio between the target and the reference object $N_{\text{BMC},t}/N_{\text{BMC},r}$ by shifting in the $\Gamma - N_{\text{BMC}}$ plot the target's pattern until it matches the reference one.
- (3) Derive the black hole mass using the following equation

$$M_{\text{BH},t} = M_{\text{BH},r} \times (N_{\text{BMC},t}/N_{\text{BMC},r}) \times (d_t/d_r)^2 \times f_G \quad (2)$$

where $M_{\text{BH},r}$ is the black hole mass of the reference object, $N_{\text{BMC},t}$ and $N_{\text{BMC},r}$ are the respective BMC normalizations for target and reference objects, d_t and d_r are the corresponding distances, and $f_G = \cos \theta_r / \cos \theta_t$ is a geometrical factor that depends on the respective inclination angles and should be included only in the scenario where the X-ray soft photon emitting region has a disk-like geometry.

Following ST09, we assume GRO J1655-40 as our primary reference source, since its system's parameters are the most tightly constrained. However, for completeness, we will consider all the reference sources and patterns used by ST09. The basic properties of these GBHs are reported in Table 1.

In Figure 1 we show the $\Gamma - N_{\text{BMC}}$ plots for our three reference sources during rise and decay phases of different outbursts (the details of these transitions are provided in ST09 and Titarchuk & Shaposhnikov 2010). Although similar at first sight, the spectral patterns differ from source to source as evidenced by the bottom right panel of Fig. 1. However, one must bear in mind that the $\Gamma - N_{\text{BMC}}$ plot yields the $N_{\text{BMC},t}/N_{\text{BMC},r}$ ratio, but the M_{BH} estimate also depends on the values of mass and distance of the reference source (see Eq. 2). As a consequence, reference sources with different patterns (and different mass and distance) may lead to similar estimates of M_{BH} (see Section 4.2).

From Figure 1 we also note that the same source displays different spectral patterns during the rise and the decay phase of an outburst. The latter behavior simply reflects the observational fact that during any outburst every GBH shows an hysteresis loop when the spectral properties (in this case the photon index Γ) are plotted versus the its intensity (here parameterized by the normalization N_{BMC}).

As outlined by ST09, when this method is utilized to estimate M_{BH} in a given GBH, one must use the appropriate reference plot. For example, a $\Gamma - N_{\text{BMC}}$ plot

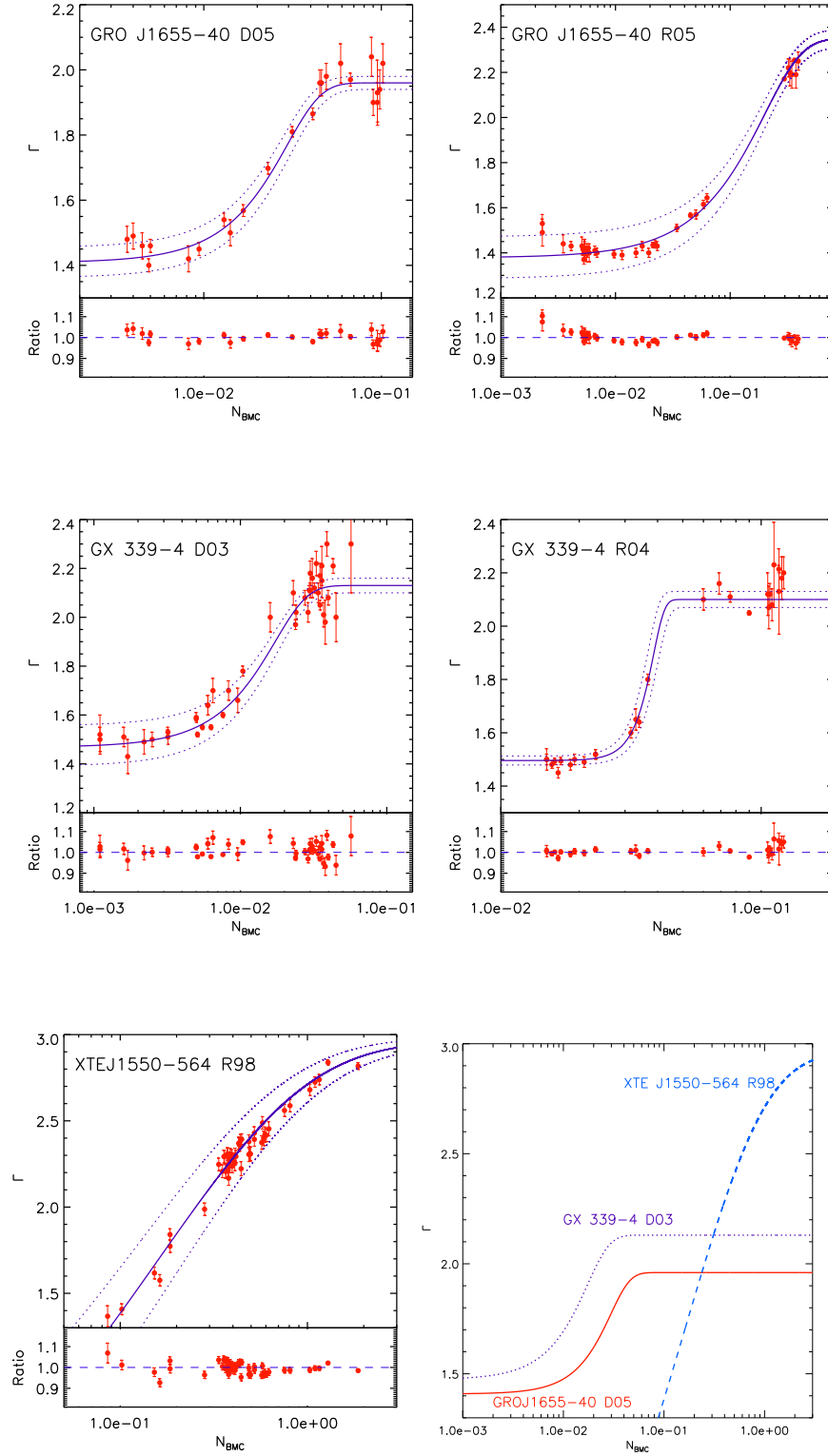


FIG. 1.— Photon index measurements plotted versus the BMC normalization values for different transitions of our three reference sources GRO J1655-40, GX 339-4, and XTE J1550-564. The thick solid line represents the best fit, whereas the dotted lines are the 1σ confidence levels. The small bottom panels describe the data-to-model ratios. Details on the fitting procedure and the values of the functional parameters are provided in the text and in Table 2. The right bottom panel shows a comparison between the spectral variability trends of the three reference sources on the same scale.

obtained during an outburst rising phase for a given target source can only be compared to a rising pattern of a suitable reference source that shows a similar trend. When applying this method to AGNs, given the much longer timescales involved, we cannot construct a complete pattern in the $\Gamma - N_{\text{BMC}}$ plot nor determine whether the AGN is in a rising or decaying outburst phase. Therefore, for completeness, we need to use all the available reference patterns and then determine which one provides the best match with the values obtained from reverberation mapping.

We fitted the X-ray spectral trends with the functional form described in Equation (1) using the Levenberg-Marquardt algorithm (Press et al. 1997). The results of the fit, which are reported in Table 2 along with the 1σ uncertainties on each parameter, are broadly consistent with those of ST09, the main difference being that in our fits all parameters are left free to vary. In this way, we can determine the uncertainty on each parameter, which is then taken into account to estimate the uncertainty on the M_{BH} values.

A priori, any of the patterns shown in Figure 1 can equally well be used to determine M_{BH} in our sample of AGNs. Indeed, all three reference sources have specific advantages: GRO J1655-40 has the best determined system parameters and therefore reduces the uncertainty associated with the estimate of M_{BH} ; GX 339-4 is known to be a prototypical GBH from the spectral variability point of view with consistent patterns in all the outbursts observed; finally, XTE J1550-564 displays the largest range of photon indices during its spectral transition, allowing to extend the estimate of M_{BH} to AGNs with steep Γ . However, a visual inspection of Figure 1 reveals that the patterns describing the outburst rise phase for the three reference sources (top and middle right panels and bottom left panel) lack the coverage of at least one part of the spectral pattern: part of the rising trend and all the upper saturation level for GRO J1655, the rising trend for GX 339-4, and both saturation levels for XTEJ1550-564. On the other hand, the decay phases of GRO J1655-40 and GX 339-4 (hereafter GRO J1655 D05 and GX 339 D03, respectively) are well-sampled across the entire range of the spectral pattern, and hence may be considered a priori more reliable. Nevertheless, only a posteriori, after a comparison of the M_{BH} estimates with the corresponding values obtained from reverberation mapping will we be able to assess which reference pattern is preferable and in which context.

3. TEST OF THE SCALING METHOD ON ACTIVE GALACTIC NUCLEI

Despite the large difference in scales, both GBHs and AGNs are believed to harbor the same central engine: a black hole and an accretion disk/corona that sometimes produces relativistic jets. There is now mounting evidence that AGNs may be considered as large-scale analogs of GBHs (see, e.g., Kording et al. 2006; McHardy et al. 2006; Sobolewska et al. 2009). Therefore, the progress made in the field of GBHs can be in principle extended to AGNs (and vice versa).

Because of their higher brightness (due to their vicinity) and their shorter variability timescales (direct consequence of their smaller M_{BH}), the temporal and spectral properties of GBHs are much better known and can be

used to infer information on their more powerful, extragalactic analogs. In the framework of the AGN-GBH unification, it thus appears reasonable to extend to AGNs the scaling method described before to determine M_{BH} .

To illustrate how this method can be extended to AGNs, in Figure 2 we show the $\Gamma - N_{\text{BMC}}$ diagram for a GBH reference source (thick solid line), and for an hypothetical AGN with $\Gamma = 1.8$ (filled circle). The only basic assumption made is that, on a much longer timescale than GBHs, the AGN follows a similar spectral pattern (light dashed line). The scaling factor necessary to obtain $M_{\text{BH,AGN}}$ starting from a reference value $M_{\text{BH,GBH}}$ is given by the product $(N_{\text{BMC,t}}/N_{\text{BMC,r}}) \times (d_t/d_r)^2$, where the first factor is determined by shifting right-ward the dashed gray (red, if printed in color) trend until it matches the solid darker one. In other words the difference in M_{BH} between the target of interest and the reference system is directly related to the amount of the shift along the x-axis in the $\Gamma - N_{\text{BMC}}$ diagram and to the square of the distance ratio.

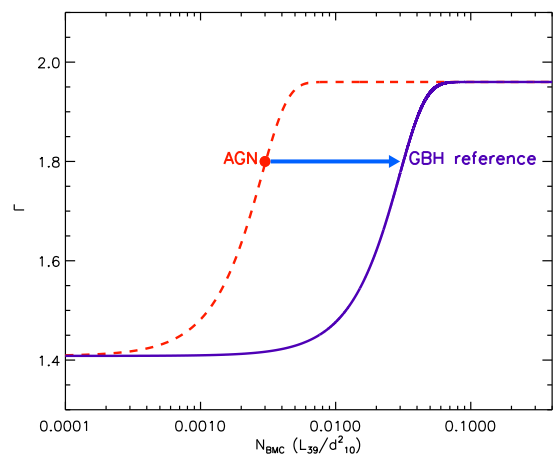


FIG. 2.— $N_{\text{BMC}} - \Gamma$ diagram for a GBH reference source and for an hypothetical AGN. The thick continuous line represents the best fitting function of the GBH spectral trend. The arrow illustrates how we determine the value of $N_{\text{BMC,t}}/N_{\text{BMC,r}}$ from the value of Γ measured for the AGN. See text for further details.

3.1. The AGN sample

We chose a sample of AGNs that fulfills two basic criteria: (1) the AGNs have BH mass estimates derived from a primary method, and (2) possess high quality X-ray data, in order to tightly constrain the parameters of the BMC model. Nearly 30 objects with M_{BH} determined via reverberation mapping by Peterson et al. (2004) have been observed by *XMM-Newton*, which, thanks to its high throughput in the 0.3–10 keV energy band, represents the best X-ray satellite for this kind of analysis.

The main properties of this sample, reported in Table 3, can be summarized as follows: the sample spans a redshift range of 0.002–0.234; the values of M_{BH} encompass nearly 3 orders of magnitude with $\log(M_{\text{BH}})$ ranging between 6.23 and 9.11 solar masses; the bolometric luminosities, computed by integrating the spectral energy distribution over the 0.001–100 keV interval by Vasudevan & Fabian (2009), span nearly 5 orders of magnitudes ranging between $4 \times 10^{42} - 1.3 \times 10^{47} \text{ erg s}^{-1}$; finally, the Eddington ratio λ_{Edd} , obtained from the ratio between bolometric and Eddington luminosity, covers

the range between 0.001–1.14. In summary, not only this AGN sample fulfills the 2 basic criteria, but also all the relevant physical parameters (with particular emphasis for M_{BH} and the Eddington ratio, which are crucial for the comparison between AGN and GBHs) span a considerably large region of the parameter space, providing the ideal framework to test the scaling method.

3.2. Data reduction

Since basically all sources are bright and with relatively large exposures (the *XMM-Newton* observation identifiers and the net exposures are reported in Table 4), we restrict our analysis to the EPIC pn data, which provide the highest S/N in the energy band of interest. The EPIC data were processed in a homogeneous way using the latest CCD gain values. For the temporal and spectral analysis, events corresponding to pattern 0–4 (singles and doubles only) were accepted. Arf and rmf files were created with the *XMM-Newton* Science Analysis Software (SAS) 8.0. The recorded events were screened to remove known hot pixels and data affected by periods of flaring background. In general, the extraction radius used for the source spectra and light curves is $30''$, whereas background spectra and light curves were extracted from source-free circular regions of $60''$ extraction radius on the same chip as the source.

The X-ray spectral analysis was performed using the XSPEC v.12.4.0 software package (Arnaud 1996). The EPIC data have been re-binned in order to contain at least 20 counts per channel for the χ^2 statistic to be valid. The errors on spectral parameters are at 90% confidence level for one interesting parameter ($\Delta\chi^2 = 2.71$).

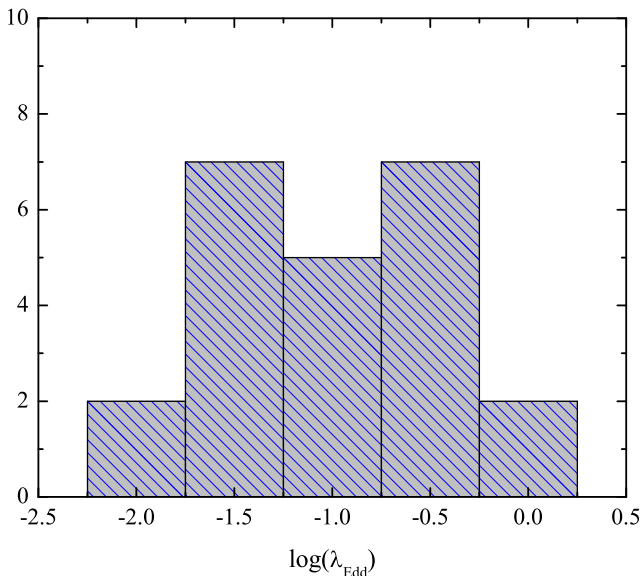


FIG. 3.— Distribution of the Eddington ratio values $\lambda_{\text{Edd}} = L_{\text{bol}}/L_{\text{Edd}}$ of the AGNs for which the M_{BH} was determined with the X-ray scaling method.

4. RESULTS

4.1. Spectral Analysis

We carried out a systematic spectral analysis of the X-ray data of all AGNs listed in Table 3 using a baseline

model that comprises a BMC model and two absorption components, one fixed at the Galactic value and one free to vary to mimic the intrinsic local absorption. When necessary, one or two Gaussian components were added to account for line-like features.

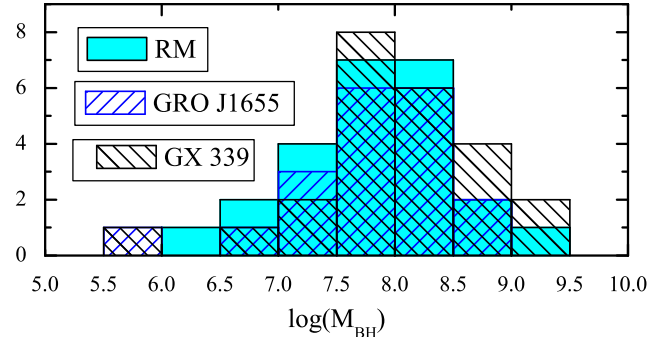


FIG. 4.— Distributions of the M_{BH} values obtained with reverberation mapping (filled histogram), and with the X-ray scaling method using as reference GRO J1655-40 D05 (dashed histogram with positive slopes) and GX 339-4 D03 (dashed histogram with negative slopes).

We restricted our analysis to the 2–10 keV energy range to avoid the complexity related to the soft X-ray band, which includes the still debated nature of the soft excess and the possible presence of warm absorbers. For completeness, we tested whether and how the estimate of M_{BH} is affected by the use of the hard X-ray data only. To this end, we first used PKS 0558–504, a bright AGN for which we have high quality proprietary *XMM-Newton* data and simultaneous coverage of the optical/UV band with the *SWIFT* UVOT (see Gliozzi et al. 2010 for details). We performed a spectral fitting analysis of both the extended optical/UV to X-ray range as well as of the restricted 2–10 keV energy band. The main difference is the resulting temperature ($kT \simeq 8 - 20$ eV when using the full range, as opposed to $kT \simeq 100$ eV obtained from the 2–10 keV band), which however has a negligible impact on the estimate of M_{BH} . The resulting values of M_{BH} differ by less than 50%. The little impact of kT (and of the parameter $\log(A)$ related to the Comptonization fraction) on the M_{BH} estimate was further assessed considering the two AGNs of our sample with the highest (Ark 120) and lowest (NGC 3227) Eddington ratio. When we arbitrarily varied by 80% the best-fit values of kT and $\log(A)$, the consequent changes of M_{BH} were of the order of 20–30% or less. We can therefore conclude that using the 2–10 keV range does not significantly affect the determination of M_{BH} for this sample of AGNs. The results of the spectral analysis are summarized in Table 4.

4.2. Estimate of M_{BH}

The estimate of M_{BH} with this scaling method crucially depends on the properties (M_{BH} , distance, and perhaps inclination angle) of the GBH primary reference sources. Although there is a general agreement on the GRO J1655-40 system parameters quoted in Table 1, it must be noted that the distance value has been questioned by Foellmi et al. (2006), who proposed a considerably smaller value ($d < 1.7$ kpc). However, it was pointed

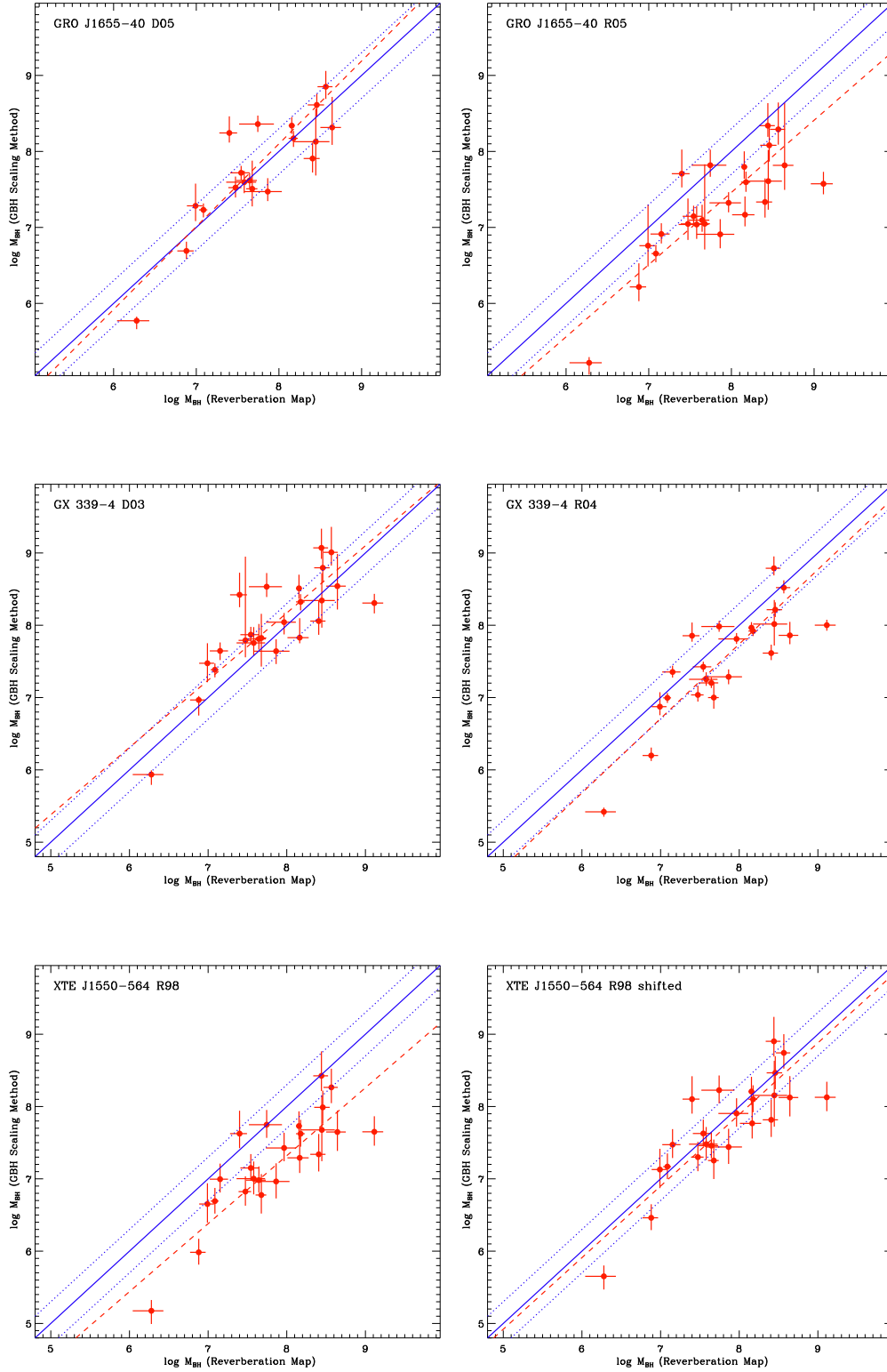


FIG. 5.— M_{BH} values obtained with the scaling method using different reference sources plotted versus the reverberation mapping values. The dashed line is the linear best-fit, the thick solid line indicates the one-to-one correlation; the dotted lines represent the 0.3 dex levels, commonly assumed as uncertainty on the reverberation mapping estimates. The geometrical factor F_G is fixed to 1 illustrating a spherical geometry scenario. In the bottom-left panels the data points have been shifted along the y axis by a factor of 3.

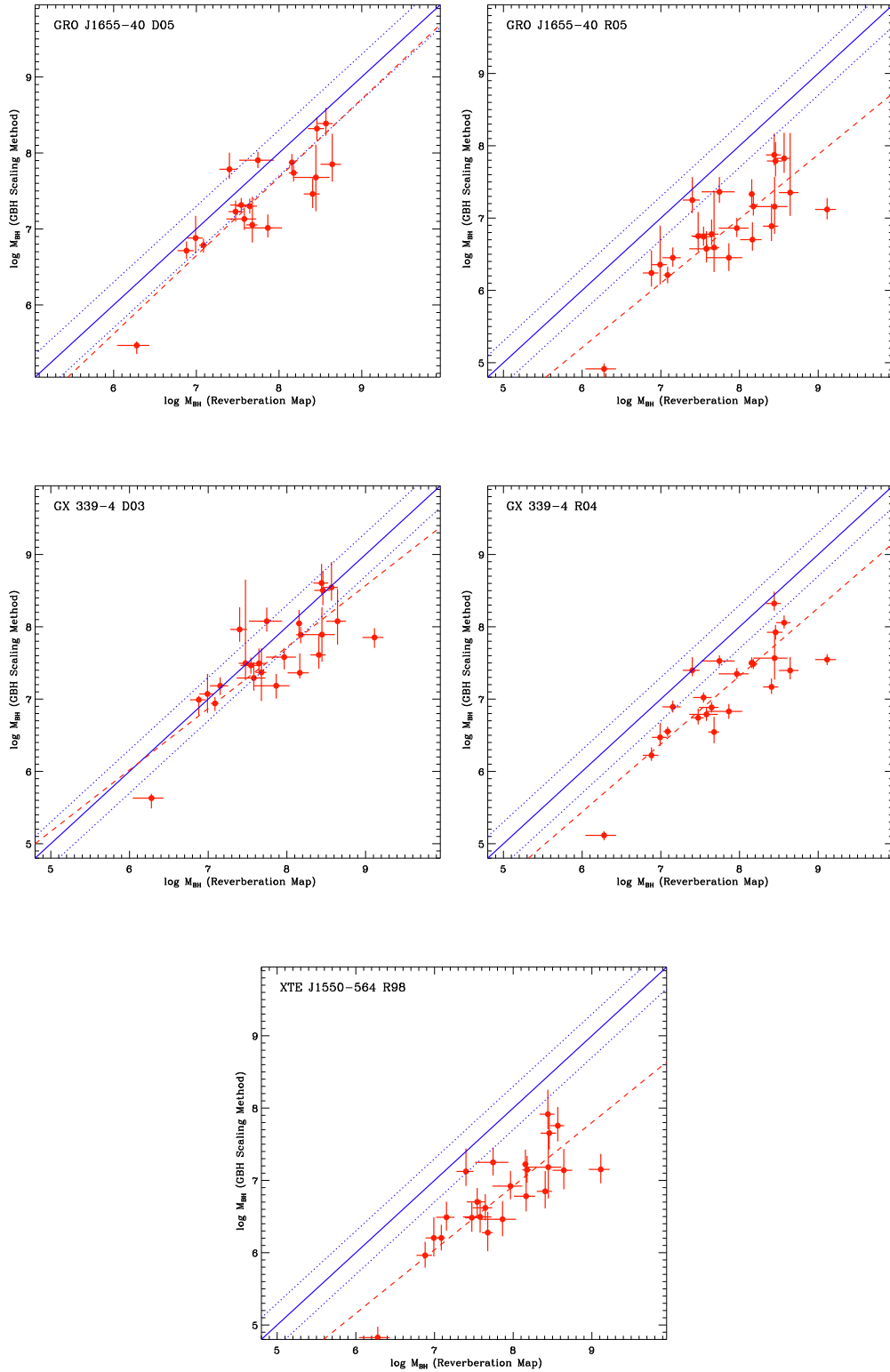


FIG. 6.— M_{BH} values obtained with the scaling method using different reference sources plotted versus the reverberation mapping values. The dashed line represents the linear best-fit, the solid line indicates the one-to-one correlation and the dashed lines are the 0.3 dex levels. The geometrical factor F_{G} is determined by the inclination angles reported in Tables 1 and 3 and illustrates a disk-like geometry.

out that the systemic velocity reported by Foellmi et al. (2006) is at odds with higher accuracy measurements reported in the literature (González Hernández et al. 2008) and that the lower value of the distance would not allow the companion star to fill its Roche lobe (Caballero García et al. 2007). In addition, the fact that using $d = 3.2$ kpc ST09 obtain an excellent agreement between the values of M_{BH} determined with the scaling technique and the corresponding dynamical values for several GBHs casts further doubts on the claim of Foellmi et al. (2006). In the remainder of the paper, we will therefore utilize for the reference sources the system parameters provided in Table 1 (if we used $d = 1.7$ kpc for GRO J1655-40 the AGN M_{BH} values would increase by a factor of ~ 3.5).

For 24 sources, the BH mass was estimated using Equation (2) and the five patterns of the reference sources shown in Fig. 1. Five objects (Mrk 79, NGC 3516, NGC 4151, PG 1226+023, and PG 1411+442), perhaps because of high intrinsic absorption and/or in reflection-dominated state, yielded photon indices too low ($\Gamma < 1.4$) to allow a direct comparison with the spectral trends of the reference sources introduced in Section 2.2. In those cases, it was not possible to determine M_{BH} with this new scaling method. The distribution of the logarithm of the Eddington ratio $\lambda_{\text{Edd}} \equiv L_{\text{bol}}/L_{\text{Edd}}$ for remaining sample is shown in Figure 3, which illustrates that λ_{Edd} spans a range of 0.01–1 with the majority of the objects populating the 0.03–0.3 interval.

Since the geometry of the X-ray emitting region is still a matter of debate, we have considered two different scenarios: (1) spherical geometry, which is defined by setting $f_G = 1$ in the M_{BH} equation, and (2) disk-like geometry where $f_G = \cos \theta_r / \cos \theta_t$ and the inclination angles given in Tables 1 and 3 are used for the reference sources (for GX 339-4 we used 70°) and the AGNs, respectively.

The distributions of the AGN M_{BH} estimates obtained from the two most well-sampled reference transitions (GRO J1655 D05 and GX 339 D03) are shown in Figure 4 along with the distribution of values from the reverberation mapping sample. The apparent general agreement between the distributions is formally confirmed by a Kolmogorov-Smirnov (KS) test, which indicates that the distributions obtained with this new X-ray scaling method are indistinguishable from the reverberation mapping one (for both reference sources the KS statistic is ~ 0.19 with an associated probability of $\sim 81\%$). We also report the individual values of M_{BH} in Table 5 to allow a direct quantitative comparison with the corresponding values from reverberation mapping. The errors quoted are computed adding in quadrature the uncertainties on the M_{BH} and distance of the reference sources (given in Table 1) and the uncertainty on the $(N_{\text{BMC,t}}/N_{\text{BMC,r}})$, which in turn depends on the 90% confidence errors of the X-ray spectral analysis on both N_{BMC} and Γ (in Table 4) as well as on the uncertainties of the functional parameters describing the reference patterns in the $\Gamma - N_{\text{BMC}}$ diagram.

The results in Table 5 suggest that this method provides M_{BH} estimates that are well constrained (with an average percentage error of $\sim 45\%$ when using the GRO J1655 D05 transition and $\sim 85\%$ for GX 339 D03) and in general agreement with the corresponding values determined via reverberation mapping (the average ratio

between the M_{BH} values determined with this method and those from reverberation mapping is 1.5 ± 0.4 for GRO J1655 D05 and 2.2 ± 0.5 for GX 339 D03).

Reasonable values for AGN M_{BH} are derived using all the reference spectral transitions available, as demonstrated by the values reported in Table 6. The 4th column of this table can be considered as the average departure from the mass ratio of 1 and hence as a proxy of the discrepancy between the values of M_{BH} determined with X-ray scaling method and the corresponding reverberation mapping ones. More specifically, $\langle \max(M_{\text{BH,ratio}}) \rangle$ is obtained by inverting the M_{BH} ratios that are lower than the unity (as an example, for Fairall 9, instead of using 0.3 as reported in columns 3 of Table 5 we use $3.3=1/0.3$) and then averaging over all M_{BH} ratios. In this way, values much lower than unity will not cancel out with values much larger than unity. The 3rd column of Table 6 reports the regular average ratio between M_{BH} values determined with the two methods. This provides information about the tendency of different reference patterns to either overestimate or underestimate M_{BH} with respect to the reverberation mapping values. For example, the spectral patterns corresponding to a decay phase of the outburst tend to slightly overestimate M_{BH} when a spherical geometry is assumed and to slightly underestimate it when a disk geometry is chosen. On the other hand, the rising patterns have a tendency to underestimate M_{BH} by a factor of $\sim 2-3$ when a spherical geometry is considered and by a larger amount when a disk-like geometry is used.

We can conclude that all the reference patterns used with a quasi-spherical illuminating soft photon emission provide reliable estimates of M_{BH} in our AGN sample, with GRO J1655 D05 and XTE J1550 R98 showing the lowest and highest average discrepancy with respect to the reverberation mapping estimates (~ 2 and ~ 6 , respectively).

4.3. Correlation Analysis

An additional direct way to compare the M_{BH} estimates from this method with the corresponding values determined via reverberation mapping is to plot one quantity versus the other and perform linear correlation tests. The M_{BH} estimates derived from all the reference transitions are plotted against the corresponding values obtained from the reverberation mapping in Figure 5 (spherical geometry) and Figure 6 (disk-like geometry), where the dashed line represents the linear best-fit, the solid line indicates the one-to-one correlation and the dotted lines are the 0.3 dex levels, commonly assumed as uncertainty on the reverberation mapping estimates. The vertical error-bars account for the uncertainties in the BH mass and distance of the reference sources, for the uncertainty of the functional reference and spectral parameters, as explained in the previous section.

A visual inspection of these figures reveals a general agreement between the M_{BH} values obtained with these two completely independent techniques. This consistency is more evident in the spherical geometry scenario shown in Figure 5. In the bottom right panel of this figure, we show that an excellent agreement can be obtained also using the XTE J1550-564 transition as a reference, provided that the M_{BH} values are systematically increased by a factor of 3. The tight correlation

observed in Figures 5 and 6 is formally confirmed by non-parametric correlation analyses based on the Spearman’s ρ and Kendall’s τ rank correlation coefficients as well as by a linear correlation fit using the routine `fitexy` (Press et al. 1997) that accounts for the errors not only on the y-axis but along the x-axis as well.

In Table 7 we report the results of this analysis. From the results of the Spearman’s and Kendall’s analyses we infer that the M_{BH} values obtained with these two different methods are always correlated at high significance level regardless of the reference transition used. This conclusion is further supported by the fact that in all cases the best-fit line’s slope is either consistent or very close to unity (and inconsistent with the zero value at more than 10σ level) and the intercept is close to zero.

5. DISCUSSION AND CONCLUSIONS

In this work, we have explored whether a new X-ray scaling method recently introduced to determine the mass of stellar black holes can be successfully extended to constrain the mass of supermassive black holes in AGNs. To this aim we have utilized a sample of 24 AGNs with $\Gamma = 1.56 - 2.11$ and $\lambda_{\text{Edd}} = 0.01 - 1$, and with M_{BH} previously determined via reverberation mapping and with good-quality archival *XMM-Newton* data. The main results can be summarized as follows.

- This novel method, which is based on the spectral fitting of X-ray data with the BMC Comptonization model and on the similarity of the X-ray spectral behavior in BHs regardless of their mass, appears to be a robust estimator of M_{BH} in AGNs.
- The values of M_{BH} determined with this method are well constrained and in good agreement (within a factor of $\sim 2-3$) with the corresponding values obtained with the reverberation mapping technique.
- For AGNs with Γ comprised in the 1.4-1.95 range the most reliable reference appears to be the outburst decay pattern of GRO J1655-40 in combination with spherical geometry (i.e., with $F_G = 1$ in Eq. 2). For $\Gamma \leq 2.1$ both decay and rise patterns of GX 339-4 and spherical geometry provide reliable estimates of M_{BH} . Finally, for steeper photon indices up to $\Gamma \sim 3$ only the rising pattern of XTE J1550-564 can be used, keeping in mind its tendency to underestimate M_{BH} by a factor of ~ 3 .
- The M_{BH} values appear to be systematically underestimated by a factor of 2-3 when a disk-like geometry is used instead of a quasi-spherical geometry for the soft photon supply. This result lends support to the hypothesis that the soft photon emission area is quasi-spherical.

In summary, our analysis reveals that this X-ray scaling technique yields black hole masses that are in full agreement with the accepted values obtained from the reverberation mapping. This is consistent with the hypothesis that the X-ray spectrum produced by the Comptonization process is self-similar and its shape is independent of M_{BH} , and lends further support to grand unification model between AGNs and GBHs.

Before concluding it is important to briefly discuss the range of applicability of this technique and its main differences with respect to most commonly used methods for black hole mass determination. First, this is one of the few truly scale-independent techniques to estimate M_{BH} . The other two scale-independent methods are the one based on the so called “fundamental plane” of black holes (BHs) introduced by Merloni et al. (2003) and Falcke et al. (2004), where M_{BH} is related to both the X-ray and radio luminosities, and the one based on the scaling of temporal breaks in X-ray power spectral density analyses (McHardy et al. 2006). However, the fundamental plane is affected by large scattering and is limited to BH systems characterized by radio emission, whereas the method based on X-ray timing requires high-quality evenly-sampled X-ray light curves spanning a baseline of more than a decade and therefore is necessarily limited to very few selected AGNs. On the other hand, this X-ray scaling novel technique only needs moderately good X-ray spectra, which are now available for a very large number of AGNs and BH systems in general. Second, unlike most indirect methods, this X-ray scaling method is completely independent of any assumption on the BLR nature/geometry or host galaxy characteristics, and can therefore complement several optically-based studies by providing independent estimates of M_{BH} , and expand them when the optical properties are uncertain or unavailable.

In principle, this technique can be applied to any accreting black hole with bulk X-ray emission produced via Comptonization and for which the photon index falls in a range covered by the GBH reference patterns in the $\Gamma - N_{\text{BMC}}$ diagram. However, we caution that a blind application of this technique may lead to erroneous results. This will occur whenever the genuine properties of the primary Comptonized X-ray emission are not properly determined, for example because effects associated with strong absorption, reflection, or emission from an additional component such as a relativistic jet are not carefully accounted for. Particular care should be used when dealing with low accreting systems, because this method has not been tested below $\lambda_{\text{Edd}} = 0.01$ and because at very low values of \dot{m} a radiatively inefficient accretion mode (possibly accompanied by outflows and jets) is likely to take place leading to the bulk of the X-rays to be dominated by jet emission as suggested by Yuan & Cui (2005).

It is also worth mentioning that AGNs are generally characterized by high flux variability, which is often accompanied by spectral variability. The vast majority of bright radio-quiet AGNs show steeper spectra when they are brighter and hence their evolution is in qualitative agreement with the rising trend in the $\Gamma - N_{\text{BMC}}$ plot, providing strong support for the physical basis of our methodology. Additionally, AGN flux and spectral changes are generally not so extreme and therefore the value obtained with different observations will be within the uncertainty of the method. Finally, occurrences of extreme spectral changes are usually associated with changing in the local obscuration component (for example from Compton-thick to Compton-thin scenario) and therefore do not reflect the intrinsic change of the Comptonized primary component. A possible notable exception is NGC 4051, which, in virtue of its small SMBH,

TABLE 1
CHARACTERISTICS OF REFERENCE SOURCES

Name	M_{BH} (M_{\odot})	d (kpc)	i (deg)
(1)	(2)	(3)	(4)
GRO J1655-40	6.3 ± 0.3	3.2 ± 0.2	70 ± 1
GX 339-4	12.3 ± 1.4	5.7 ± 0.8	> 45
XTE J1550-564	10.7 ± 1.5	3.3 ± 0.5	72 ± 5

Columns Table 1: 1= Source name. 2= Black hole mass. 3= Distance. 4= Inclination angle. **Notes:** For GRO J1655-40 the quoted values of M_{BH} , d , and i are from Greene et al. (2001) and Hjellming & Rupen (1995). For both GX 339-4 and XTE J1550-564 M_{BH} and d are from ST09, whereas the values of i are respectively from from Kolehmainen & Done (2010) and from Orosz et al. (2002).

shows extreme flux and spectral changes that might reflect genuine changes of the primary X-ray component. This is indeed the only source for which a complete trend in the $\Gamma - N_{\text{BMC}}$ plot can be constructed. Preliminary results based on numerous *XMM-Newton* and *Chandra* observations suggest that NGC 4051 follow a trend consistent with GBH references and that the scaling method successfully determine its mass (Chekhtman & Titarchuk 2011, in preparation).

In the near future, we plan to systematically apply this X-ray scaling method to different categories of objects, whose M_{BH} values are currently debated, such as

ultraluminous X-ray sources, narrow line Seyfert 1 galaxies, non-jet-dominated radio loud AGNs, and powerful quasars to test the upper end of the $M_{\text{BH}} - \sigma_{\star}$ relationship.

We thank the anonymous referee for constructive suggestions that have improved the clarity of the paper. We thank Nikolai Shaposhnikov for providing the spectral data of XTE J1550-564 and for useful discussions. MG acknowledges support by the NASA ADP grant NNXIOAD51G.

REFERENCES

- Arnaud, K. 1996, in ASP Conf. Ser. 101, *Astronomical Data Analysis Software and Systems V*, ed. G. Jacoby & J. Barnes (San Francisco: ASP), 17
- Bian, W. & Zhao, Y. 2002, *A&A*, 395, 465
- Caballero Garcia et al. 2007, *ApJ*, 669, 534
- Constantin, A., Green, P., Aldcroft, T., Kim, D.-W., Haggard, D., Barkhouse, W., & Anderson, S.F. 2009, *ApJ*, 705, 1336
- Czerny, B. & Nikolajuk, M. 2010, *MmSAI*, 81, 281 (astro-ph:0910.0313)
- Denney, K.D. et al. 2010, *ApJ*, 721, 715
- Fabian, A.C., Sanders, J.S., Taylor, G.B., & Allen, S.W. 2003, *MNRAS*, 360, L20
- Falcke, H., Körding, E., & Markoff, S. 2004, *A&A*, 414, 895
- Ferrarese, L. & Merritt, D. 2000, *ApJ*, 539, 9
- Foellmi, C., depagne, E., Dall, T.H., & Mirabel, I.F. 2006, *A&A*, 457, 249
- Gebhardt, K., et al. 2000, *ApJ*, 539, L13
- Gierliński, M., Middleton, M., Ward, M., & Done, C. 2008, *Nature*, 455, 369
- Gliozzi, M., et al. 2010, *ApJ*, 717, 1243
- González Hernández, J.I., Rebolo, R., & Israelian, G. 2008, *A&A*, 478, 203
- Greene, J., Bailyn, C.D., & Orosz, J.A. 2001, *ApJ*, 554, 1290
- Grier, C.J., et al. 2008, *ApJ*, 688, 837
- Hjellming, R.M. & Rupen, M.P. 1995, *Nature*, 375, 464
- Kolehmainen, M. & Done, C. 2010, *MNRAS*, 406, 2206
- Körding, E.G., Jester, S., & Fender, R.P. 2006, *MNRAS*, 372, 1366
- Kormendy, J. & Richstone, D. 1995, *ARA&A*, 33, 581
- Magorrian, J., et al. 1998, *AJ*, 115, 2285
- Maiolino, R. & Rieke, G.H. 1995, *ApJ*, 454, 95
- McHardy, I.M., Körding, E.G., Knigge, C., Uttley, P., & Fender, R.P. 2006, *Nature*, 444, 730
- McNamara, B.R., et al. 2000, *ApJ*, 534, L135
- Merloni, A., Heinz, S., & di Matteo, T. 2003, *MNRAS*, 345, 1057
- Orosz, J.A., et al. 2002, *ApJ*, 568, 8450
- Papadakis, I.E., et al. 2009, *A&A*, 494, 905
- Peterson, B.M., et al. 2004, *ApJ*, 613, 682
- Press, W.H., Teukolsky, S.A., Vetterling, W.T., & Flannery, B.P. 1997, *Numerical Recipes* (Cambridge: Cambridge Univ. Press)
- Shaposhnikov, N. & Titarchuk, L. 2009, *ApJ*, 699, 453 (ST09)
- Shemmer, O., Brandt, W.N., Netzer, H., Maiolino, R., & Kaspi, S. 2006, *ApJ*, 646, L29
- Sobolewska, M.A., Gierliński, M., & Siemiginowska, A. 2009, *MNRAS*, 394, 1640
- Spergel, D.N., et al. 2003, *ApJS*, 148, 175
- Titarchuk, L.G., Mastichiadis, A. & Kylafis, N.D. 1997, *ApJ*, 487, 834
- Titarchuk, L. & Shaposhnikov, N. 2010, *ApJ*, 724, 1147
- Vasudevan, R.V. & Fabian, A.C. 2009, *MNRAS*, 392, 1124
- Vestergaard, M. 2009, Invited contribution to the 2007 Spring Symposium on "Black Holes" at the Space Telescope Science Institute (astro-ph:0904.2615)
- Wu, Q. & Gu, M. 2008, *ApJ*, 682, 212
- Yuan, F. & Cui, W. 2005, *ApJ*, 629, 408

TABLE 2
PARAMETRIZATION OF $\Gamma - N_{\text{BMC}}$ REFERENCE PATTERNS

Transition (1)	A (2)	B (3)	N_{tr} (4)	β (5)	χ_r^2 (dof) (6)
GRO J1655 D05	1.96 ± 0.02	0.42 ± 0.02	0.023 ± 0.001	1.8 ± 0.2	1.5 (20)
GRO J1655 R05	2.35 ± 0.04	0.74 ± 0.04	0.131 ± 0.001	1.0 ± 0.1	1.8 (34)
GX339 D03	2.13 ± 0.03	0.50 ± 0.04	0.0130 ± 0.0002	1.5 ± 0.3	0.9 (40)
GX339 R04	2.10 ± 0.03	0.46 ± 0.01	0.037 ± 0.001	8.0 ± 1.5	2.3 (24)
XTE J1550 R98	2.96 ± 0.02	2.8 ± 0.2	0.055 ± 0.010	0.4 ± 0.1	2.7 (49)

Columns Table 2: 1= Reference source spectral transition. 2= Parameter of the functional form described in Eq.(1) that is responsible for the rigid translation of the spectral pattern along the y-axis. 3= Parameter characterizing the lower saturation level of the pattern. 4= Parameter responsible for the translation of the spectral pattern along the x-axis. 5= Slope of the spectral pattern. 6= Reduced χ^2 and degrees of freedom. **Notes:** The quoted parameter errors are the 1σ uncertainties obtained from fitting the spectral data using the Levenberg-Marquardt algorithm.

TABLE 3
SAMPLE PROPERTIES

Name	z	(i) (deg)	$\log(M_{\text{BH}})$ (M_{\odot})	$\log(L_{\text{bol}})$ (erg s^{-1})	λ_{Edd} ($L_{\text{bol}}/L_{\text{Edd}}$)
(1)	(2)	(3)	(4)	(5)	(6)
3C 120	0.0330	13^{+11}_{-6}	7.74	45.3	0.305
3C 390.3	0.0561	48^{+24}_{-20}	8.46	45.2	0.047
Ark 120	0.0327	22^{+16}_{-9}	8.18	45.3	0.111
Fairall 9	0.0470	17^{+13}_{-7}	8.41	44.8	0.019
Mrk 110	0.0353	11^{+9}_{-5}	7.40	45.1	0.433
Mrk 279	0.0305	30	7.54	45.0	0.210
Mrk 335	0.0258	8^{+6}_{-4}	7.15	45.3	1.130
Mrk 509	0.0344	5^{+4}_{-2}	8.16	45.2	0.095
Mrk 590	0.0264	13^{+9}_{-6}	7.68	43.8	0.010
Mrk 79	0.0222	31^{+23}_{-13}	7.72	44.3	0.031
NGC 3227	0.0039	71^{+17}_{-24}	6.88	42.9	0.001
NGC 3516	0.0088	30	7.50	43.5	0.006
NGC 3783	0.0097	48^{+27}_{-21}	7.47	44.2	0.043
NGC 4051	0.0023	46^{+27}_{-20}	6.23	42.6	0.016
NGC 4151	0.0033	77^{+10}_{-22}	7.12	44.0	0.056
NGC 4593	0.0090	30	6.99	43.7	0.037
NGC 5548	0.0172	45^{+23}_{-18}	7.65	44.3	0.024
NGC 7469	0.0163	18^{+13}_{-8}	7.09	44.8	0.369
PG 0052+251	0.1550	5^{+4}_{-2}	8.57	45.8	0.148
PG 0844+349	0.0640	8^{+6}_{-3}	7.97	45.4	0.233
PG 0953+414	0.2341	2^{+2}_{-1}	8.44	46.5	0.892
PG 1211+143	0.0809	3^{+2}_{-1}	8.16	45.7	0.260
PG 1226+023	0.1583	1^{+1}_{-1}	8.95	47.1	1.140
PG 1229+204	0.0630	12^{+10}_{-5}	7.86	44.9	0.082
PG 1307+085	0.1550	5^{+5}_{-2}	8.64	45.6	0.066
PG 1411+442	0.0896	3^{+2}_{-1}	8.65	45.4	0.041
PG 1426+015	0.0865	13^{+11}_{-6}	9.11	45.6	0.024
PG 1613+658	0.1290	15^{+12}_{-7}	8.45	45.9	0.221
PG 2130+099	0.0630	6^{+4}_{-3}	7.58	45.0	0.018

Columns Table 3: 1= Source name. 2= Redshift. 3= Inclination angle. 4= Black hole mass determined via reverberation mapping. 5= Bolometric luminosity. 6= Eddington ratio. **Notes:** The AGN distances were computed from z assuming $H_0 = 71 \text{ km s}^{-1} \text{ Mpc}^{-1}$, $\Omega_{\Lambda} = 0.73$, and $\Omega_m = 0.27$ (Spergel et al. 2003). For nearby AGNs we used the redshift-independent distances provided by the NASA/IPAC extragalactic database (NED). The quoted values of the inclination angle are from Bian & Zhao (2002); for objects without estimate of inclination angle (Mrk 279, NGC 3516, NGC 4593) we assumed a value of 30° typical for Seyfert galaxies. M_{BH} values are from Peterson et al. (2004) with the exception of NGC 3227, NGC 3516, NGC 4051, NGC 5548 (Denney et al. 2010), and PG 2130+099 (Grier et al. 2008). Values for (L_{bol}) and λ_{Edd} are from Vasudevan & Fabian (2009).

TABLE 4
SPECTRA RESULTS

Name	XMM obsid	Net exposure (ks)	kT (keV)	$Log(A)$	Γ	N_{BMC} (10^{-4})	χ_r^2 (dof)
(1)	(2)	(3)	(4)	(5)	(6)	(7)	(8)
3C 120	0152840101	79.1	0.4 ± 0.1	0.7 ± 0.1	$1.69^{+0.02}_{-0.02}$	$4.5^{+0.1}_{-0.1}$	1.02(1211)
3C 390.3	0203720201	35.0	0.1 ± 0.1	0.7	$1.66^{+0.04}_{-0.03}$	$2.5^{+0.2}_{-0.2}$	1.13(817)
Ark 120	0147190101	55.9	0.4 ± 0.4	0.5 ± 0.1	$1.84^{+0.03}_{-0.03}$	$4.2^{+0.1}_{-0.1}$	1.07(1000)
Fairall 9	0101040201	26.0	0.1 ± 0.1	0.5 ± 0.1	$1.80^{+0.07}_{-0.10}$	$1.0^{+0.1}_{-0.1}$	1.05(866)
Mrk 110	0201130501	32.9	0.3 ± 0.1	0.6 ± 0.3	$1.68^{+0.03}_{-0.02}$	$2.7^{+1.0}_{-0.1}$	0.99(1290)
Mrk 279	0302480501	34.9	0.05	0.95	$1.80^{+0.01}_{-0.01}$	$1.5^{+0.1}_{-0.1}$	1.05(1252)
Mrk 335	0306870101	83.3	0.3 ± 0.1	0.4 ± 0.1	$1.98^{+0.03}_{-0.03}$	$2.2^{+0.2}_{-0.1}$	0.99(1364)
Mrk 509	0306090401	44.9	0.3 ± 0.1	0.6 ± 0.1	$1.69^{+0.02}_{-0.02}$	$4.1^{+0.1}_{-0.1}$	1.02(1468)
Mrk 590	0201020201	39.5	0.4 ± 0.1	0.8 ± 0.2	$1.54^{+0.05}_{-0.11}$	$0.6^{+0.1}_{-0.1}$	1.03(838)
Mrk 79	0502091001	49.0	0.11	0.7	$1.22^{+0.02}_{-0.02}$	$0.4^{+0.1}_{-0.1}$	1.02(1065)
NGC 3227	0400270101	96.1	0.08	0.5	$1.56^{+0.003}_{-0.003}$	$2.9^{+0.1}_{-0.1}$	0.98(1574)
NGC 3516	0107460701	81.8	0.2 ± 0.1	0.5	$1.32^{+0.02}_{-0.01}$	$1.3^{+0.1}_{-0.1}$	1.06(1411)
NGC 3783	0112210501	89.5	0.2 ± 0.1	0.8	$1.56^{+0.01}_{-0.01}$	$4.2^{+0.2}_{-0.2}$	1.19(1325)
NGC 4051	0606320101	45.7	0.1 ± 0.1	0.1 ± 0.1	$1.72^{+0.004}_{-0.004}$	$1.5^{+0.1}_{-0.1}$	0.99(1059)
NGC 4151	0143500301	12.4	0.01	2.0	$1.35^{+0.01}_{-0.01}$	$3.4^{+0.1}_{-0.1}$	1.30(1593)
NGC 4593	0109970101	5.0	0.4 ± 0.1	0.6 ± 0.2	$1.65^{+0.08}_{-0.09}$	$3.6^{+0.4}_{-0.4}$	0.94(648)
NGC 5548	0089960301	50.5	0.10	0.6 ± 0.1	$1.64^{+0.01}_{-0.01}$	$2.5^{+0.1}_{-0.1}$	1.01(1494)
NGC 7469	0207090101	58.3	0.2 ± 0.1	1.2	$1.86^{+0.01}_{-0.01}$	$2.0^{+0.1}_{-0.1}$	1.15(902)
PG 0052+251	0301450401	8.2	0.3 ± 0.2	0.5	$1.75^{+0.08}_{-0.11}$	$0.6^{+0.1}_{-0.1}$	0.93(243)
PG 0844+349	0103660201	12.7	0.3 ± 0.1	0.4 ± 0.4	$2.00^{+0.12}_{-0.14}$	$0.6^{+0.9}_{-0.1}$	0.96(297)
PG 0953+414	0111290201	11.2	0.1 ± 0.1	0.1	$2.00^{+0.07}_{-0.11}$	$0.5^{+0.1}_{-0.1}$	0.74(170)
PG 1211+143	0502050101	45.6	0.1 ± 0.1	2.0	$2.11^{+0.03}_{-0.03}$	$0.4^{+0.2}_{-0.1}$	0.90(659)
PG 1226+023	0414190101	45.7	0.10	0.5	$1.39^{+0.01}_{-0.01}$	$6.4^{+0.1}_{-0.1}$	1.04(1595)
PG 1229+204	0301450201	16.9	0.05	1.0	$1.91^{+0.06}_{-0.06}$	$0.3^{+0.1}_{-0.1}$	0.94(253)
PG 1307+085	0110950401	10.6	0.10	0.6	$1.60^{+0.10}_{-0.09}$	$0.1^{+0.1}_{-0.1}$	0.91(98)
PG 1411+442	0103660101	22.4	0.07	2.0	$1.00^{+1.00}_{-1.00}$	$3.4^{+0.3}_{-0.3}$	0.92(41)
PG 1426+015	0102040501	5.4	0.03	1.2	$1.97^{+0.06}_{-0.06}$	$0.4^{+0.1}_{-0.1}$	0.88(214)
PG 1613+658	0102040601	5.0	0.04	1.2	$1.94^{+0.29}_{-0.26}$	$0.3^{+0.3}_{-0.1}$	1.05(14)
PG 2130+099	0150470701	21.9	0.06	0.7	$1.73^{+0.05}_{-0.05}$	$0.2^{+0.1}_{-0.1}$	0.98(339)

Columns Table 4: 1= Source name. 2= *XMM-Newton* observation identifier. 3= EPIC pn net exposure time in ks. 4= Temperature of thermal photon source in keV. 5= Logarithm of the A parameter, which is related to the Comptonization fraction f by the relation $f = A/(1 + A)$. 6= 2–10 keV photon index. 7= Normalization of the Comptonization model in units of $(L/10^{39} \text{ erg s}^{-1})(10 \text{ kpc}/d)^2$. 8= Reduced χ^2 and degrees of freedom. **Notes:** In the cases, where the **error** procedure in **XSPEC** was not able to provide the 90% confidence uncertainty for kT or $\log(A)$ due to low S/N data or spectral degeneracy, we fixed the parameters at their best-fit value. The upper limit of $\log(A)$ was fixed at the value of 2.

TABLE 5
BLACK HOLE MASS ESTIMATES

Name (1)	GRO J1655 D05				GX 339 D03			
	Sphere		Disk		Sphere		Disk	
	$\log M_{\text{BH}}$ (2)	scal/RM (3)	$\log M_{\text{BH}}$ (4)	scal/RM (5)	$\log M_{\text{BH}}$ (6)	scal/RM (7)	$\log M_{\text{BH}}$ (8)	scal/RM (9)
3C 120	8.36 ± 0.17	4.1	7.91 ± 0.17	1.4	8.53 ± 0.21	6.1	8.08 ± 0.21	2.2
3C 390.3	8.61 ± 0.20	1.4	8.32 ± 0.20	0.7	8.80 ± 0.27	2.2	8.50 ± 0.27	1.1
Ark 120	8.17 ± 0.16	1.0	7.74 ± 0.16	0.4	8.32 ± 0.17	1.4	7.89 ± 0.17	0.5
Fairall 9	7.91 ± 0.24	0.3	7.46 ± 0.24	0.1	8.06 ± 0.27	0.5	7.61 ± 0.27	0.2
Mrk 110	8.24 ± 0.29	7.0	7.78 ± 0.29	2.4	8.42 ± 0.28	10.5	7.96 ± 0.28	3.7
Mrk 279	7.71 ± 0.25	1.5	7.32 ± 0.25	0.6	7.87 ± 0.17	2.1	7.47 ± 0.17	0.8
Mrk 335	7.65 ± 0.18	3.1	7.18 ± 0.18	1.1
Mrk 509	8.34 ± 0.17	1.5	7.89 ± 0.17	0.5	8.51 ± 0.21	2.3	8.05 ± 0.21	0.8
Mrk 590	7.51 ± 0.34	0.7	7.04 ± 0.34	0.2	7.82 ± 0.40	1.4	7.37 ± 0.40	0.5
NGC 3227	6.69 ± 0.17	0.6	6.24 ± 0.17	0.2	6.97 ± 0.20	1.2	6.99 ± 0.20	1.3
NGC 3783	7.52 ± 0.19	1.1	7.55 ± 0.19	1.2	7.79 ± 0.73	2.1	7.50 ± 0.73	1.1
NGC 4051	5.77 ± 0.15	0.3	5.48 ± 0.15	0.2	5.94 ± 0.17	0.5	5.63 ± 0.17	0.2
NGC 4593	7.28 ± 0.28	2.0	6.98 ± 0.28	1.0	7.47 ± 0.31	3.0	7.07 ± 0.31	1.2
NGC 5548	7.62 ± 0.16	0.9	7.21 ± 0.16	0.4	7.81 ± 0.22	1.5	7.49 ± 0.22	0.7
NGC 7469	7.23 ± 0.16	1.4	6.91 ± 0.16	0.7	7.39 ± 0.16	2.0	6.94 ± 0.16	0.7
PG 0052+251	8.85 ± 0.23	1.9	8.41 ± 0.23	0.7	9.01 ± 0.31	2.8	8.54 ± 0.31	1.0
PG 0844+349	8.04 ± 0.20	1.2	7.58 ± 0.20	0.4
PG 0953+414	9.07 ± 0.25	4.3	8.61 ± 0.25	1.5
PG 1211+143	7.83 ± 0.22	0.5	7.36 ± 0.22	0.2
PG 1229+204	7.47 ± 0.20	0.4	7.01 ± 0.20	0.1	7.64 ± 0.22	0.6	7.18 ± 0.22	0.2
PG 1307+085	8.32 ± 0.35	0.5	7.85 ± 0.35	0.2	8.54 ± 0.42	0.8	8.08 ± 0.42	0.3
PG 1426+015	8.31 ± 0.19	0.2	7.85 ± 0.19	0.1
PG 1613+658	8.13 ± 0.48	0.5	7.66 ± 0.48	0.2	8.34 ± 0.41	0.8	7.89 ± 0.41	0.3
PG 2130+099	7.60 ± 0.20	1.0	7.58 ± 0.20	0.4	7.76 ± 0.24	1.5	7.29 ± 0.24	0.5

Columns Table 5: 1= Source Name. 2= M_{BH} in solar units computed using the GRO J1655 D05 transition in the case of spherical geometry. 3= Ratio between the M_{BH} in column 2 and the corresponding value determined via reverberation mapping. 4= Same as column 2 but for a disk-like geometry. 5= Ratio between the M_{BH} in column 3 and the corresponding value determined via reverberation mapping. 6= M_{BH} in solar units computed using the GX 339 D03 transition in the case of spherical geometry. 7= Ratio between the M_{BH} in column 6 and the corresponding value determined via reverberation mapping. 8= Same as column 6 but for a disk-like geometry. 9= Ratio between the M_{BH} in column 8 and the corresponding value determined via reverberation mapping. **Notes:** For five sources (Mrk 335, PG 0844+349, PG 0953+414, PG 1211+143, PG 1426+015), the photon index is too steep ($\Gamma > 1.96$) to determine M_{BH} using the decay phase of GRO J1655-40.

TABLE 6
STATISTICAL ANALYSIS RESULTS

Transition (1)	Geometry (2)	$\langle M_{\text{BH,scal}}/M_{\text{BH,RM}} \rangle$ (3)	$\langle \max(M_{\text{BH,ratio}}) \rangle$ (4)
GRO D05	Sphere	1.5 ± 0.4	2.2 ± 0.3
	Disk	0.6 ± 0.1	3.3 ± 0.5
GRO R05	Sphere	0.4 ± 0.1	5.7 ± 1.4
	Disk	0.16 ± 0.03	14.9 ± 4.1
GX D03	Sphere	2.2 ± 0.5	2.7 ± 0.4
	Disk	0.8 ± 0.2	3.1 ± 0.7
GX R04	Sphere	0.7 ± 0.1	3.3 ± 0.6
	Disk	0.3 ± 0.1	7.7 ± 1.7
XTE R98	Sphere	0.4 ± 0.1	5.8 ± 1.2
	Sphere-shift	1.1 ± 0.2	2.5 ± 0.4
	Disk	0.13 ± 0.02	16.6 ± 3.8

Columns Table 6: 1= Reference source spectral transition. 2= Geometry of the soft photon emission region. 3= Ratio of the M_{BH} values determined with the scaling method over the corresponding values from the reverberation mapping averaged over the entire sample. 4= Maximum average ratio of the M_{BH} values which provides an estimate of the average discrepancy (see Section 4.2 for details). **Notes:** The “sphere-shift” case corresponds to the spherical corona scenario where the M_{BH} values obtained from the scaling technique have been multiplied by a factor of 3. The large values of $\langle \max(M_{\text{BH,ratio}}) \rangle$ for patterns corresponding to rising phase outbursts (especially in the cases of disk geometry) reflect the systematic underestimate of M_{BH} not the true departure from the black hole mass ratio of 1.

TABLE 7
CORRELATION ANALYSIS RESULTS

Transition (1)	Geom. (2)	Slope (3)	Intercept (4)	Spearman (Prob.) (5)	Kendall (Prob.) (6)
GRO D05	Sphere	1.09 ± 0.07	-0.6 ± 0.6	$0.78 (9 \times 10^{-5})$	$0.59 (4 \times 10^{-4})$
	Disk	1.03 ± 0.06	-0.6 ± 0.5	$0.77 (1 \times 10^{-4})$	$0.57 (5 \times 10^{-4})$
GRO R05	Sphere	0.95 ± 0.07	-0.1 ± 0.5	$0.78 (5 \times 10^{-6})$	$0.62 (2 \times 10^{-5})$
	Disk	0.89 ± 0.07	-0.1 ± 0.5	$0.77 (1 \times 10^{-5})$	$0.59 (6 \times 10^{-5})$
GX D03	Sphere	0.93 ± 0.08	0.7 ± 0.6	$0.79 (4 \times 10^{-6})$	$0.63 (2 \times 10^{-5})$
	Disk	0.85 ± 0.07	0.9 ± 0.6	$0.76 (1 \times 10^{-5})$	$0.58 (7 \times 10^{-5})$
GX R04	Sphere	1.03 ± 0.07	-0.5 ± 0.5	$0.84 (5 \times 10^{-7})$	$0.65 (1 \times 10^{-5})$
	Disk	0.94 ± 0.06	-0.2 ± 0.5	$0.82 (2 \times 10^{-6})$	$0.64 (2 \times 10^{-5})$
XTE R98	Sphere	0.97 ± 0.09	-0.4 ± 0.7	$0.80 (2 \times 10^{-6})$	$0.62 (2 \times 10^{-5})$
	Sphere-shift	0.99 ± 0.08	-0.03 ± 0.6
	Disk	0.88 ± 0.09	-0.1 ± 0.7	$0.80 (2 \times 10^{-6})$	$0.62 (2 \times 10^{-5})$

Columns Table 7: 1= Reference source spectral transition. 2= Geometry of the soft photon emission region. 3= Best-fit slope obtained fitting the data in Figures 3 and 4 with a straight line. 4= Best-fit intercept. 5= Spearman’s ρ rank correlation coefficient and related chance probability. 6= Kendall’s τ rank correlation coefficient and related chance probability. **Notes:** The quoted parameter errors for slope and intercept account for the uncertainties on both x and y. The uncertainty on the average mass ratio represents the spread around the mean $\sqrt{\sigma/n}$, where n is the number of AGNs. For the “sphere-shift” case the values of the Spearman and Kendall analyses have been omitted since they coincide with those of the “sphere” case.